

JOURNAL OF GLACIOLOGY



CAMBRIDGE
UNIVERSITY PRESS

THIS MANUSCRIPT HAS BEEN SUBMITTED TO THE JOURNAL OF GLACIOLOGY AND HAS NOT BEEN PEER-REVIEWED.

Reconstructing subglacial lake activity with an altimetry-based inverse method

Journal:	<i>Journal of Glaciology</i>
Manuscript ID	Draft
Manuscript Type:	Article
Date Submitted by the Author:	n/a
Complete List of Authors:	Stubblefield, Aaron; Dartmouth College, Thayer School of Engineering Meyer, Colin; Dartmouth College, Thayer School of Engineering Siegfried, Matthew; Colorado School of Mines, Department of Geophysics Sauthoff, Wilson; Colorado School of Mines, Hydrologic Science and Engineering Spiegelman, Marc; Lamont-Doherty Earth Observatory, Earth and Environmental Science; Columbia University, Applied Physics and Applied Mathematics
Keywords:	Subglacial lakes, Antarctic glaciology, Subglacial processes, Ice-sheet modelling
Abstract:	Subglacial lake water-volume changes produce ice-elevation anomalies that provide clues about water flow beneath glaciers and ice sheets. Significant challenges remain in the quantitative interpretation of these elevation-change anomalies because the surface expression of subglacial lake activity depends on basal conditions, rate of water-volume change, and ice rheology. To address these challenges, we introduce an inverse

	<p>method that reconstructs subglacial lake activity from altimetry data while accounting for the effects of viscous ice flow. We use a linearized approximation of a Stokes ice-flow model under the assumption that subglacial lake activity only induces small perturbations relative to a reference ice-flow state. We validate this assumption by accurately reconstructing lake activity from synthetic data that are produced with a fully nonlinear model. We then apply the method to estimate the water-volume changes of several active subglacial lakes in Antarctica by inverting data from NASA's Ice, Cloud, and land Elevation Satellite 2 (ICESat-2) laser altimetry mission. The results show that there can be substantial discrepancies (20% or more) between the inversion and traditional estimation methods due to the effects of viscous ice flow. The inverse method will help refine estimates of subglacial water transport and further constrain the role of subglacial hydrology in ice-sheet evolution.</p>

SCHOLARONE™
Manuscripts

Reconstructing subglacial lake activity with an altimetry-based inverse method

Aaron G. STUBBLEFIELD,¹ Colin R. MEYER,¹ Matthew R. SIEGFRIED,^{2,3} Wilson SAUTHOFF,³ Marc SPIEGELMAN^{4,5}

¹*Thayer School of Engineering, Dartmouth College, Hanover, NH, USA*

²*Department of Geophysics, Colorado School of Mines, Golden, CO, USA*

³*Hydrologic Science and Engineering, Colorado School of Mines, Golden, CO, USA*

⁴*Lamont-Doherty Earth Observatory, Columbia University, Palisades, NY, USA*

⁵*Department of Applied Physics and Applied Mathematics, Columbia University, New York, NY, USA*

<aaron.g.stubblefield@dartmouth.edu>

ABSTRACT. Subglacial lake water-volume changes produce ice-elevation anomalies that provide clues about water flow beneath glaciers and ice sheets. Significant challenges remain in the quantitative interpretation of these elevation-change anomalies because the surface expression of subglacial lake activity depends on basal conditions, rate of water-volume change, and ice rheology. To address these challenges, we introduce an inverse method that reconstructs subglacial lake activity from altimetry data while accounting for the effects of viscous ice flow. We use a linearized approximation of a Stokes ice-flow model under the assumption that subglacial lake activity only induces small perturbations relative to a reference ice-flow state. We validate this assumption by accurately reconstructing lake activity from synthetic data that are produced with a fully nonlinear model. We then apply the method to estimate the water-volume changes of several active subglacial lakes in Antarctica by inverting data from NASA's Ice, Cloud, and land Elevation Satellite 2 (ICESat-2) laser altimetry mission. The results show that there can be substantial discrepancies (20% or more) between the inversion and traditional estimation methods due to the effects of viscous ice flow. The inverse method will help

28 **refine estimates of subglacial water transport and further constrain the role of**
29 **subglacial hydrology in ice-sheet evolution.**

30 INTRODUCTION

31 Ice-sheet surface elevation responds to a variety of time-varying subglacial phenomena, including subglacial-
32 lake volume change, basal-drag variations, and melting or freezing at the ice-water interface. Active sub-
33 glacial lakes (i.e., those that experience observable volume change in the observational record) in particular
34 have received much attention due to the localized perturbations they produce in ice-sheet surface elevation
35 during volume-change events (e.g., Gray and others, 2005; Wingham and others, 2006; Fricker and oth-
36 ers, 2007). NASA's Ice, Cloud, and land Elevation Satellite (ICESat) and the European Space Agency's
37 CryoSat-2 satellite altimetry missions facilitated the detection of over one hundred active subglacial lakes
38 beneath the Antarctic Ice Sheet (e.g., Smith and others, 2009; Wright and Siegert, 2012; Fricker and others,
39 2016; Livingstone and others, 2022), driving investigations into their possible relation to fast ice flow (e.g.,
40 Stearns and others, 2008; Scambos and others, 2011; Siegfried and others, 2016) and into their ability to
41 host microbial ecosystems (e.g., Christner and others, 2014; Achberger and others, 2016; Davis and others,
42 2023). Fewer subglacial lakes have been discovered beneath the Greenland Ice Sheet based on ice-surface
43 changes, suggesting that there may be significant differences in subglacial hydrological conditions there
44 relative to the Antarctic Ice Sheet (e.g., Bowling and others, 2019; Livingstone and others, 2019, 2022).

45 High-resolution satellite altimetry data from NASA's ICESat-2 mission presents a valuable opportunity
46 to continue investigating dynamic conditions beneath ice sheets (e.g., Markus and others, 2017; Neckel and
47 others, 2021; Siegfried and Fricker, 2021). Modelling has shown that accurately estimating subglacial-lake
48 volume change, areal extent, and highstand or lowstand timing from altimetry alone can be complicated by
49 the effects of viscous ice flow (Stubblefield and others, 2021a). Basal vertical velocity anomalies associated
50 with subglacial lake activity can manifest with a wider areal extent and smaller amplitude at the ice-
51 sheet surface when ice flows laterally towards or away from the lake during volume-change events. Ice
52 viscosity, ice thickness, and basal drag exert strong control on ice flow and, therefore, also influence the
53 surface expression of subglacial lake activity (Stubblefield and others, 2021a). Although satellite altimetry
54 data has been incorporated in basal-drag inversions (e.g., Larour and others, 2014; Arthern and others,
55 2015; Goldberg and others, 2015; Mosbeux and others, 2016), inverse methods that quantify subglacial-lake

56 activity from altimetry and account for ice-flow effects have not yet been developed.

57 Inversion of time-varying altimetry data necessitates leveraging reduced-order models to alleviate the
58 computational cost associated with repeatedly solving the forward problem. Dimensionality reduction
59 is often achieved using ice-flow models that are based on depth-integrated approximations of the Stokes
60 equations (e.g., Greve and Blatter, 2009). Solving the linearized Stokes equations on simplified domains
61 with spectral methods is an alternative way to achieve computational efficiency when the full stresses in the
62 ice must be resolved (e.g., Budd, 1970; Hutter and others, 1981; Balise and Raymond, 1985; Gudmundsson,
63 2003; Sergienko, 2012). Previous inversions relying on perturbation methods have not included time-varying
64 data (Gudmundsson and Raymond, 2008; Thorsteinsson and others, 2003). Likewise, a computational
65 method for inverting time-varying elevation data with perturbation-based models would be a valuable step
66 towards quantifying time-varying subglacial lake perturbations. We use this small-perturbation approach
67 as subglacial lake activity only induces small perturbations in ice-surface elevation (i.e., $O(1\text{ m})$) relative
68 to ice thickness.

69 Here, we derive, test, and apply an altimetry-based inverse method for quantifying basal vertical ve-
70 locity perturbations that arise from subglacial lake activity. First, we outline the forward model for the
71 perturbation in ice-surface elevation that is produced by a basal vertical velocity forcing. We then derive the
72 inverse method from a least-squares optimization problem. To verify and validate the method, we present
73 tests with synthetic data from both the linearized and nonlinear models. We then apply the method to a
74 collection of active subglacial lakes in Antarctica (Figure 1). The results show that ice flow can produce
75 significant discrepancies between the inverse method and a traditional altimetry-based estimation method
76 for calculating changes in subglacial water volume over the current ICESat-2 time period. We conclude by
77 discussing limitations, extensions, and further applications of the method.

78 METHOD

79 In this section, we derive the forward model and the associated inverse method. First, we outline the
80 general Stokes flow problem to highlight the governing equations and simplifying assumptions. Then, we
81 outline a derivation of the small-perturbation model that is used in the inverse method. Finally, we derive
82 the inverse method with a least-squares optimization approach.

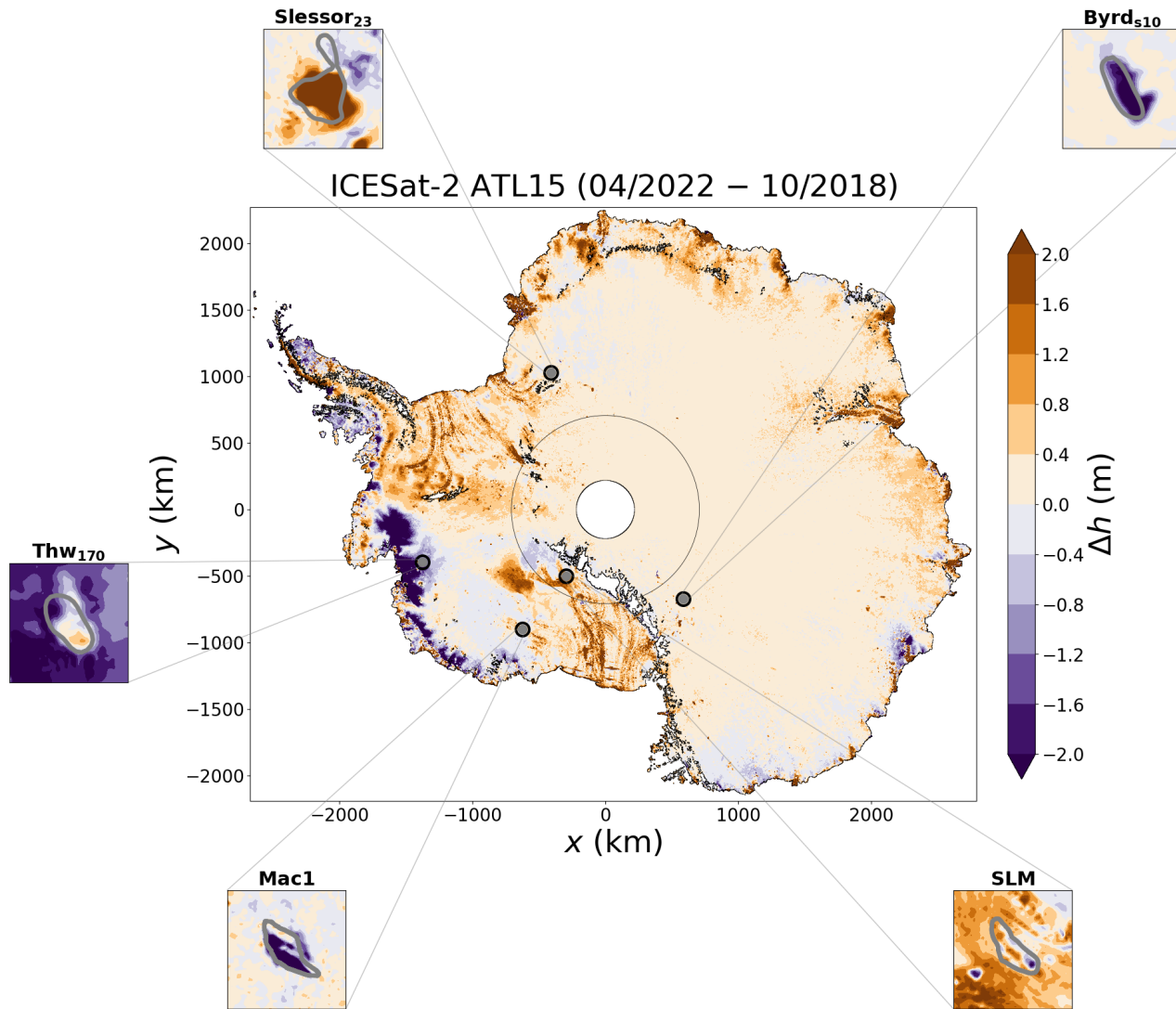


Fig. 1. Map of ICESat-2 ATL15 gridded product (Smith and others, 2022) showing the elevation change of the Antarctic Ice Sheet between October 2018 and April 2022. Insets show the locations of the subglacial lakes targeted as examples in this study. Subglacial lake boundaries derived from surface altimetry are shown as gray lines (Siegfried and Fricker, 2018). Regional thinning occurs around Thwaites Lake 170 (Thw₁₇₀) and regional thickening occurs around Mercer Subglacial Lake (SLM). Regional elevation-change trends around Slessor Glacier (lake Slessor₂₃), MacAyeal Ice Stream (lake Mac1), and Byrd Glacier (lake Byrd_{s10}) are less pronounced. We remove regional trends to produce elevation-change anomalies that are used in the inversions.

83 **Stokes flow**

84 We assume that ice deforms as a viscous fluid according to the incompressible Stokes equations, which are
85 given by

$$-\nabla \cdot \boldsymbol{\sigma} = \rho_i \mathbf{g} \quad (1)$$

$$\nabla \cdot \mathbf{u} = 0, \quad (2)$$

86 where ρ_i is the ice density, \mathbf{u} is the ice velocity, and $\mathbf{g} = g[0, 0, -1]^T$ denotes gravitational acceleration with
87 magnitude g . The stress tensor $\boldsymbol{\sigma}$ is defined via

$$\boldsymbol{\sigma} = -p\mathbf{I} + \eta (\nabla \mathbf{u} + \nabla \mathbf{u}^T) \quad (3)$$

88 where p is the pressure, \mathbf{I} is the identity tensor, and η is the viscosity. At the ice-bed boundary we assume
89 a sliding law of the form

$$\mathbb{T}\boldsymbol{\sigma}\mathbf{n} = -\beta\mathbb{T}\mathbf{u} \quad (4)$$

90 where β is the basal drag coefficient, \mathbf{n} is an outward-pointing unit normal to the boundary, and $\mathbb{T} = \mathbf{I} - \mathbf{n}\mathbf{n}^T$
91 is a projection tangential to the ice-sheet surface. Although the small-perturbation model used in the
92 inversions assumes a Newtonian viscosity and linear sliding law (i.e., constant η and β), we will also consider
93 synthetic data produced by a fully nonlinear model with Glen's law viscosity (Glen, 1955) and a nonlinear
94 Weertman-style sliding law (Weertman, 1957) to test the validity of these simplifications (Stubblefield and
95 others, 2021b).

96 The upper surface of the ice-sheet $z = h(x, y, t)$ evolves over time according to the kinematic equation

$$\frac{\partial h}{\partial t} + u \frac{\partial h}{\partial x} + v \frac{\partial h}{\partial y} = w \quad (5)$$

97 where the velocity components are evaluated at the surface ($z = h$). We assume that a stress-free condition

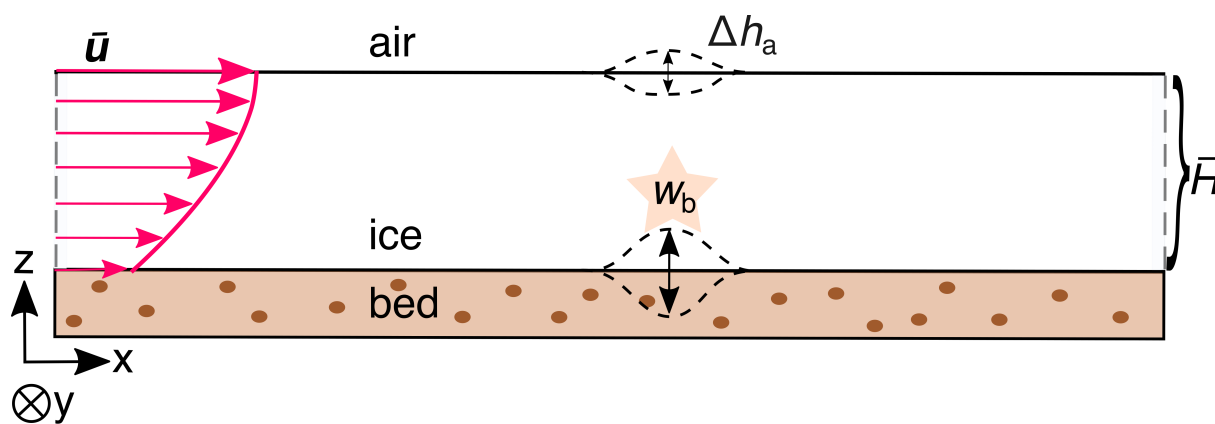


Fig. 2. Sketch of linearized model setup. The horizontal (map-plane) coordinates are (x, y) with the y direction pointing into the page. The basal vertical velocity anomaly w_b produces an elevation-change anomaly Δh_a . The ice thickness is \bar{H} and the horizontal surface velocity is \bar{u} in the reference flow state. The ice flow is aligned with the x axis here for simplicity but generally also has a component in the y direction.

$$\sigma n = 0 \quad (6)$$

98 holds at the upper surface of the ice sheet. We approximate the spatial domain as a horizontally unbounded
 99 slab because the ice-sheet extent is much greater than areal extent of the subglacial lakes. Away from the
 100 lake, we assume that all quantities approach an appropriate far-field reference state that is based on data
 101 and available ice-sheet model output.

102 Small-perturbation model

103 Now we will describe the forward model that is used in the inverse method. Although small-perturbation
 104 models have been derived previously, we outline a derivation here to highlight the assumptions underlying
 105 the inverse method (Balise and Raymond, 1985; Gudmundsson, 2003). Our goal is to find the basal vertical
 106 velocity perturbation w_b that produces the surface elevation-change anomaly Δh_a under the assumption
 107 that these anomalies arise from subglacial lake activity (Figure 2). We could also incorporate a basal drag
 108 anomaly to represent a slippery spot over a lake in the small-perturbation framework (e.g., Gudmundsson,
 109 2003; Stubblefield, 2022), but the resulting dipolar elevation-change anomaly (Sergienko and others, 2007)
 110 is not discernible in any of the active lakes considered herein. We revisit this idea in the discussion.

111 To derive a simplified model for this system, we assume that Δh_a and w_b are small perturbations from
 112 a known reference state that is (approximately) characterized by a constant ice thickness \bar{H} , horizontal

113 surface velocity $\bar{\mathbf{u}} = [\bar{u}, \bar{v}]^T$, ice viscosity $\bar{\eta}$, and basal drag coefficient $\bar{\beta}$. We further assume that the basal
 114 surface is horizontal in the reference state and that the ice pressure equals the cryostatic pressure. Strictly
 115 speaking, an advective component is only present in the free-slip limit ($\bar{\beta} = 0$) under the assumption of
 116 a horizontally uniform Stokes flow over a flat bed subject to the stress boundary conditions (4) and (6).
 117 However, we retain a background advective velocity in all cases for consistency with the data.

118 Letting $[u_h, v_h, w_h]^T$ denote the perturbation in ice-sheet surface velocity, we insert perturbations to
 119 the reference states, $h = \bar{H} + \Delta h_a$ and $\mathbf{u} = [\bar{u}, \bar{v}, 0]^T + [u_h, v_h, w_h]^T$, into the kinematic equation (5) to
 120 obtain

$$\frac{\partial \Delta h_a}{\partial t} + \bar{u} \frac{\partial \Delta h_a}{\partial x} + \bar{v} \frac{\partial \Delta h_a}{\partial y} = w_h. \quad (7)$$

121 We have neglected terms involving products of perturbations in (7) under the assumption of small per-
 122 turbations. We solve equation (7) by taking Fourier transforms with respect to the horizontal coordinates
 123 (x, y) to obtain

$$\frac{\partial \widehat{\Delta h_a}}{\partial t} + (i\mathbf{k} \cdot \bar{\mathbf{u}}) \widehat{\Delta h_a} = \widehat{w}_h, \quad (8)$$

124 where $\mathbf{k} = [k_x, k_y]^T$ is the horizontal wavevector. The vertical surface velocity is assumed to satisfy the
 125 Stokes flow problem (1)-(6), subject to the above simplifications, which allows us to derive a closed-form
 126 expression of the solution operator (Balise and Raymond, 1985; Gudmundsson, 2003; Stubblefield and
 127 others, 2021a).

128 We algebraically solve the Fourier-transformed Stokes problem to obtain an expression for the trans-
 129 formed vertical surface velocity,

$$\widehat{w}_h = -\mathcal{R} \widehat{\Delta h_a} + \mathcal{T} \widehat{w}_b, \quad (9)$$

130 in terms of the basal vertical velocity and surface elevation anomalies (e.g., Stubblefield and others, 2021a,
 131 Supporting Information). In equation (9), \mathcal{R} is a relaxation function that controls the decay rate of the
 132 elevation anomaly, and \mathcal{T} is a transfer function that maps the basal vertical velocity anomaly to its surface
 133 expression. These functions depend on the scaled wavevector magnitude $k' = |\mathbf{k}| \bar{H}$ and drag coefficient

134 $\gamma = \bar{\beta}\bar{H}/(2\bar{\eta}k')$ through the relations

$$\mathcal{R} = \left(\frac{\rho_i g \bar{H}}{2\bar{\eta}k'} \right) \frac{(1 + \gamma)e^{4k'} - (2 + 4\gamma k')e^{2k'} + 1 - \gamma}{(1 + \gamma)e^{4k'} + (2\gamma + 4k' + 4\gamma k'^2)e^{2k'} - 1 + \gamma}, \quad (10)$$

135 and

$$\mathcal{T} = \frac{2(1 + \gamma)(k' + 1)e^{3k'} + 2(1 - \gamma)(k' - 1)e^{k'}}{(1 + \gamma)e^{4k'} + (2\gamma + 4k' + 4\gamma k'^2)e^{2k'} - 1 + \gamma}. \quad (11)$$

136 For a detailed derivation of the expressions (10) and (11) see, for example, Stubblefield and others (2021a,
137 Supporting Information) and Stubblefield (2022, Appendix E).

138 Substituting the expression (9) into (8), we find that the ice-surface elevation anomaly Δh_a evolves in
139 frequency space via

$$\frac{\partial \widehat{\Delta h}_a}{\partial t} + (i\mathbf{k} \cdot \bar{\mathbf{u}})\widehat{\Delta h}_a = -\mathcal{R}\widehat{\Delta h}_a + \mathcal{T}\widehat{w}_b. \quad (12)$$

140 The solution to equation (12) is given by

$$\widehat{\Delta h}_a = \widehat{\Delta h}_0 e^{-(i\mathbf{k} \cdot \bar{\mathbf{u}} + \mathcal{R})t} + \widehat{w}_b * \mathcal{K} \quad (13)$$

141 where $*$ denotes convolution over time and Δh_0 is the elevation perturbation at the initial time $t = 0$. The
142 kernel \mathcal{K} , defined by

$$\mathcal{K} = \mathcal{T} e^{-(i\mathbf{k} \cdot \bar{\mathbf{u}} + \mathcal{R})t}, \quad (14)$$

143 controls the decay of the elevation-change anomaly and transfer of the basal anomaly to the surface. The
144 characteristic time scale for the decay of surface-elevation anomalies is

$$t_{\text{relax}} = \frac{2\bar{\eta}}{\rho_i g \bar{H}}, \quad (15)$$

145 which controls the magnitude of the relaxation function \mathcal{R} (cf. Turcotte and Schubert, 2002, Chapter 6).

146 The effects of viscous ice flow influence the surface expression of lake activity when the viscous relaxation

147 time t_{relax} is comparable to the lake filling or draining timescale (Stubblefield and others, 2021a). We
 148 highlight the importance of the viscous relaxation time in the examples below.

149 Inverse method

150 Now we will outline the inverse method. We let F denote the (map-plane) Fourier transform operator and
 151 define the relative elevation-change anomaly via

$$d = \Delta h_a - F^{-1} \left(e^{-(i\mathbf{k} \cdot \bar{\mathbf{u}} + \mathcal{R})t} F(\Delta h_0) \right), \quad (16)$$

152 which has the contribution from the initial value in equation (13) removed. From equation (13), we define
 153 the operator G that maps w_b to the relative elevation change d via

$$G(w_b) = F^{-1}(F(w_b) * \mathcal{K}) \quad (17)$$

154 where the kernel \mathcal{K} is defined in equation (14).

155 We consider a regularized least-squares objective functional,

$$J(w_b) = \frac{1}{2} \int_0^{t_f} \int_{-\infty}^{+\infty} \int_{-\infty}^{+\infty} |G(w_b) - d|^2 dx dy dt + \frac{\varepsilon}{2} \int_0^{t_f} \int_{-\infty}^{+\infty} \int_{-\infty}^{+\infty} |\nabla w_b|^2 dx dy dt, \quad (18)$$

156 where t_f is the final time and the parameter ε controls the strength of the regularization term. While the
 157 regularization in (18) promotes smoothness, other regularizations could be chosen to promote sparsity of
 158 the basal forcing, for example (Stadler, 2009). The minimizer of the objective (18) satisfies the normal
 159 equation

$$G^*(G(w_b)) - \varepsilon \nabla^2 w_b = G^*(d), \quad (19)$$

160 which can be derived with variational calculus (Vogel, 2002; Hanke, 2017). The adjoint operator G^* in (19)
 161 is given by

$$G^*(f) = F^{-1}(F(f) \star \mathcal{K}) \quad (20)$$

162 for any function f , where \star denotes cross-correlation over time.

163 We solve the equation (19) with the conjugate gradient method to obtain the basal vertical velocity
 164 w_b . In using the conjugate gradient method to solve this operator equation, we avoid explicitly con-
 165 structing matrices corresponding to the forward and adjoint operators, and instead simply require the
 166 action of these operators on functions (Atkinson and Han, 2009, Section 5.6). We implemented the dis-
 167 cretized inverse method in Python with SciPy’s fast Fourier transform and convolution algorithms (Virta-
 168 nen and others, 2020). The code is openly available and will be archived with Zenodo prior to publication
 169 (<https://github.com/agstub/lake-altimetry-inversions>).

170 Estimation of water-volume change

171 To compare the inversion with previous estimation methods, we will focus on estimating subglacial water-
 172 volume changes. Given the basal vertical velocity inversion w_b , the basal water-volume change over a
 173 map-plane area B can be computed via

$$\Delta V_{\text{inv}}(t) = \int_0^t \left[\iint_B w_b \, dx \, dy \right] dt'. \quad (21)$$

174 Alternatively, the volume-change has often been estimated in previous studies by integrating the elevation
 175 change anomaly over the static outline of a lake (Fricker and Scambos, 2009; Smith and others, 2009).
 176 Using this approach, the water-volume change is estimated by

$$\Delta V_{\text{alt}}(t) = \iint_B \Delta h_a - \Delta h_0 \, dx \, dy, \quad (22)$$

177 where we have integrated over the same map-plane area B . Although an alternative lake boundary could
 178 be identified with the inversion, we use the same boundary to calculate both estimates for consistency in
 179 comparison. We revisit this problem in the discussion.

180 In the limits $\mathcal{R} \rightarrow 0$ and $\mathcal{T} \rightarrow 1$, equation (12) implies that these volume changes are equivalent (i.e.,
 181 $\Delta V_{\text{inv}} = \Delta V_{\text{alt}}$). This “rigid-ice” limit is approached when the ice is viscous enough for the relaxation
 182 timescale, t_{relax} (eq. 15), to greatly exceed the volume-change timescale (Stubblefield and others, 2021a).
 183 Although incompressibility causes these volume changes to be equal when integrating over the entire areal
 184 extent of a glacier, this approach is impractical for the Antarctic Ice Sheet due to the presence of multiple
 185 lakes and regional thickening or thinning trends. We explore the discrepancy between the inversion-derived

186 estimate (21) and surface-derived estimate (22) for a range of parameters in the examples below.

187 SYNTHETIC EXAMPLES

188 Before applying the method to the ICESat-2 altimetry data, we first solve two problems with synthetic data
189 to verify and validate the method. First, we verify the implementation by inverting synthetic data that is
190 produced by prescribing the linearized model with a known basal vertical velocity field and then adding
191 Gaussian white noise to the resulting elevation change. For consistency with the ICESat-2 examples, we
192 remove a small off-lake elevation-change component, Δh_{off} , from the elevation change as detailed in the
193 next section. For this example, we choose a basal vertical velocity field that is a Gaussian bump undergoing
194 sinusoidal oscillations in time. The inverse method is able to reconstruct the basal vertical velocity and
195 volume-change time series from the synthetic data (Figure 3). We find that there is little deviation ($\lesssim 5\%$)
196 between the volume change estimates (21) and (22) on short timescales (i.e., less than ~ 2.5 years), whereas
197 large deviations occur over decadal timescales. This behavior arises because the viscosity is $\bar{\eta} = 10^{15}$ Pa s
198 for this example, leading to characteristic relaxation timescale of $t_{\text{relax}} \approx 2.8$ yr. These results highlight that
199 Antarctic subglacial lakes will not show significant deviations over the current ICESat-2 time period if the
200 ice viscosity reaches this magnitude. We provide an example of this behavior below. In all examples herein,
201 we set the regularization parameter to $\varepsilon = 1$ in equation (19), which results in accurate reconstructions of
202 the synthetic examples without over-fitting the data.

203 Next, we show an example with synthetic data produced by a fully nonlinear model to test the assump-
204 tions underlying the small-perturbation approach (Stubblefield and others, 2021b,a). The nonlinear model
205 assumes a Glen's law viscosity (Glen, 1955; Cuffey and Paterson, 2010), a nonlinear Weertman-style sliding
206 law (Weertman, 1957), fully nonlinear surface kinematic equations, and vanishing basal drag over the lake.
207 For this example, we have assumed radial symmetry with respect to the map-plane coordinates (x, y) to
208 facilitate numerical solution in three spatial dimensions. We also prescribe a more complex volume-change
209 time series to produce the synthetic data (Figure 4). Despite the simplifications inherent to the inverse
210 method, the inversion accurately recovers the volume change time series that is produced by the nonlinear
211 model (Figure 4). Most importantly, the inversion is much more accurate than the surface-based volume
212 change for this parameter regime. The examples in Figure 3 and Figure 4 show that the altimetry-based
213 estimate tends to underestimate the magnitude of the true water volume change, regardless of whether the
214 volume change is positive or negative. Next, we describe the data and preprocessing steps before discussing

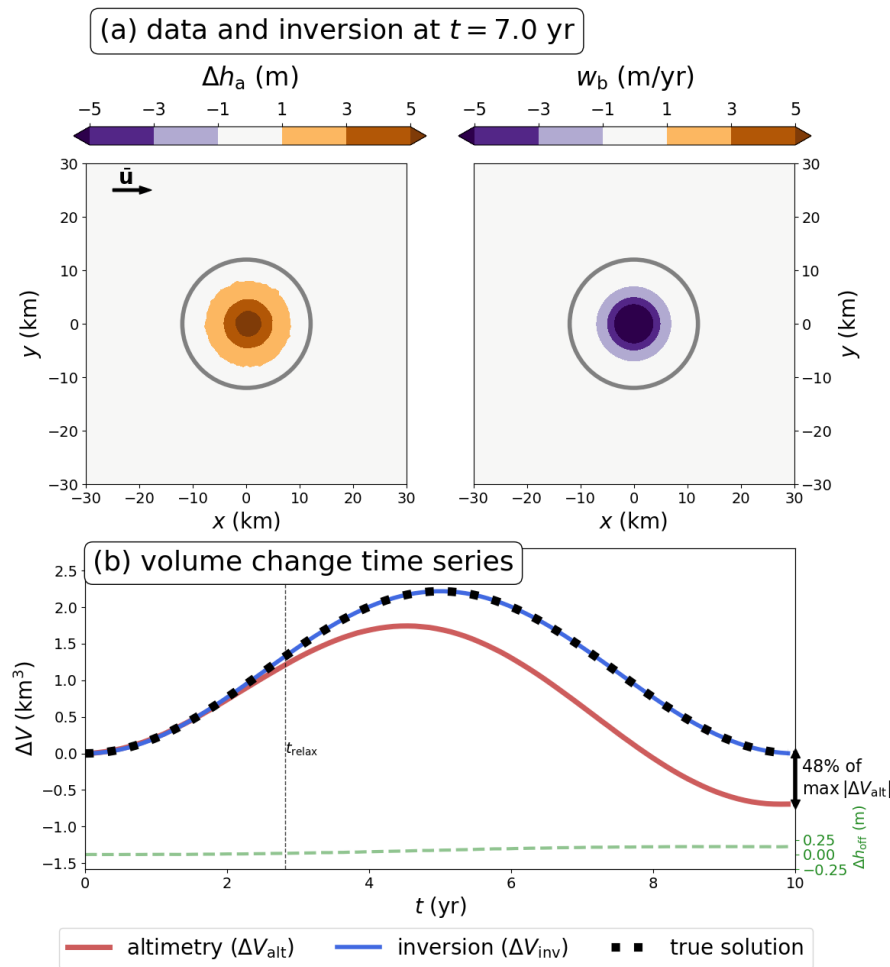


Fig. 3. Inversion results for synthetic data produced with the linearized model. (a) Map-plane elevation anomaly and inversion at $t = 7$ yr. (b) Time series of the surface-derived volume change (ΔV_{alt}), the inversion-based volume change (ΔV_{inv}), and the off-lake component (Δh_{off}) that is removed prior to inversion. The gray contours in (a) and (b) show the boundaries used to compute the volume-change time series. The ice flow direction is shown by the black arrow in (a). The maximum deviation between the surface-derived volume change and the inversion in (b) is 0.83 km^3 , or 48% of the maximum amplitude of the surface-derived estimate. The inversion accurately recovers the true water-volume change (dashed black line). The parameters for this example are $\bar{H} = 2500 \text{ m}$, $\bar{\eta} = 10^{15} \text{ Pa s}$, $\bar{\beta} = 10^{11} \text{ Pa s m}^{-1}$, $\bar{u} = 200 \text{ m yr}^{-1}$, and $\bar{v} = 0 \text{ m yr}^{-1}$. The viscous relaxation time associated with these parameters is $t_{\text{relax}} = 2.82 \text{ yr}$. See Movie S1 for an animation of the inversion over all time steps.

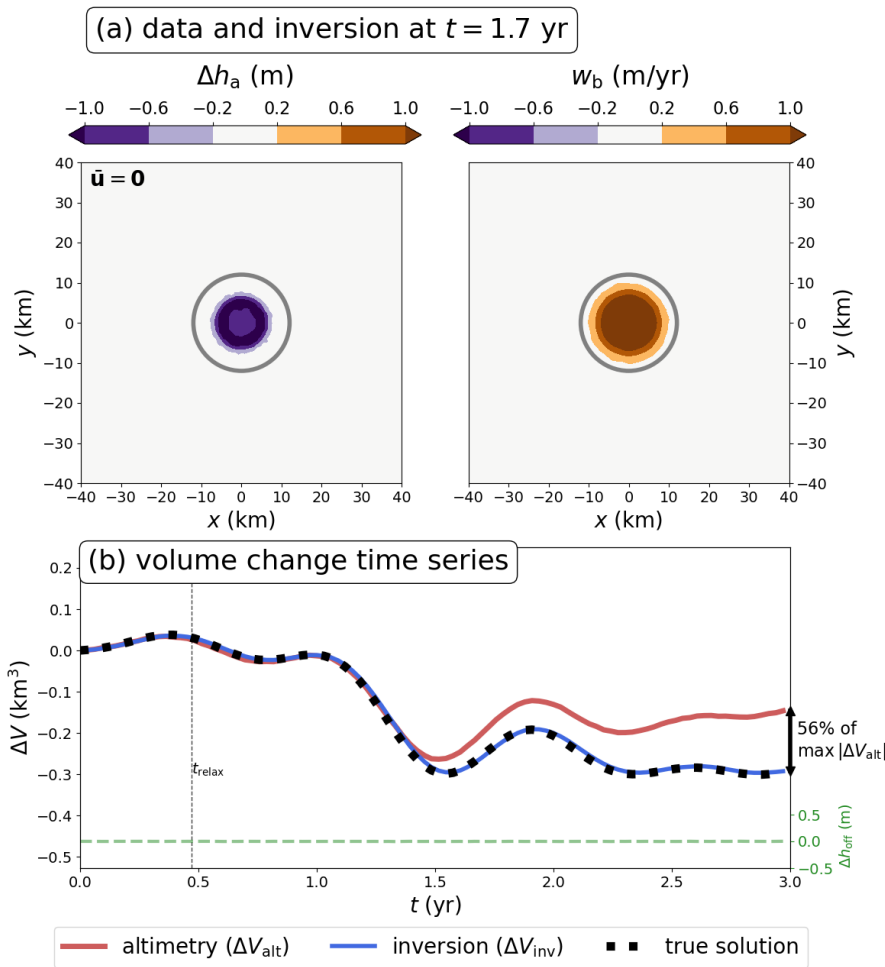


Fig. 4. Inversion results for synthetic data produced with a radially-symmetric nonlinear Stokes model (Stubblefield and others, 2021b). (a) Map-plane elevation anomaly and inversion at $t = 1.7$ yr. (b) Time series of the surface-derived volume change (ΔV_{alt}), the inversion-based volume change (ΔV_{inv}), and the off-lake component (Δh_{off}) that is removed prior to inversion. The gray contours in (a) and (b) show the boundaries used to compute the volume-change time series. The maximum deviation between the surface-derived volume change and inversion in (b) is 0.15 km^3 , or 56% of the maximum amplitude of the surface-derived estimate. The inversion accurately recovers the true water-volume change (dashed black line). The parameters for this example are $\bar{H} = 1500 \text{ m}$, $\bar{\eta} = 10^{14} \text{ Pa s}$, $\bar{\beta} = 10^{10} \text{ Pa s m}^{-1}$, $\bar{u} = 0 \text{ m yr}^{-1}$, and $\bar{v} = 0 \text{ m yr}^{-1}$. The viscous relaxation time associated with these parameters is $t_{\text{relax}} = 0.47 \text{ yr}$. See Movie S2 for a detailed animation of the nonlinear model and Movie S3 for an animation of the inversion over all time steps.

215 examples of ICESat-2 inversions.

216 DATA AND PREPROCESSING

217 We use the ICESat-2 ATL15 L3B Gridded Antarctic and Arctic Land Ice Height Change (Version 2) data
 218 product (Smith and others, 2022) to obtain elevation-change anomalies above the Antarctic subglacial
 219 lakes shown in Figure 1. For the examples explored here, we interpolated the ICESat-2 ATL15 data onto
 220 a space-time grid with 100 points in each direction (t, x, y) to obtain the same resolution as the numerical
 221 model. Alternatively, we could restrict the model-data misfit in (18) to the discrete set of data points, but
 222 this could require additional temporal regularisation that we have not included in this study. We remove
 223 any regional thickening or thinning trends by subtracting the spatially averaged off-lake component, Δh_{off} ,
 224 as described below. We also have to establish a reference elevation profile to define the elevation-change
 225 anomaly. By default, the elevation changes in ATL15 are relative to the ice-surface elevation on January
 226 1, 2020. In general, the elevation anomaly can be defined relative to any of the ATL15 time points by
 227 subtracting the elevation surface at a particular reference time t_{ref} . Therefore, the elevation change anomaly
 228 is derived from the ATL15 elevation change product Δh via

$$\Delta h_{\text{a}}(x, y, t) = \Delta h(x, y, t) - \Delta h_{\text{off}}(t) - [\Delta h(x, y, t_{\text{ref}}) - \Delta h_{\text{off}}(t_{\text{ref}})] \quad (23)$$

229 where Δh_{off} is the (time-varying) spatial average of Δh away from the lake. Here, the spatial average is
 230 taken over all points that are at a distance greater than 80% from the centroid of the lake to the boundary
 231 of the computational domain.

232 Based on previously identified lake activity, an appropriate reference time t_{ref} to define the anomalies
 233 happens to be the initial time in the ATL15 product, October 1, 2018, for all of the lakes considered here
 234 except Mercer Subglacial Lake (SLM). SLM reached an apparent highstand near the end of 2017 before
 235 beginning a drainage event during the ICESat-2 period (Siegfried and Fricker, 2021), so the initial time
 236 in the ICESat-2 data does not correspond to an elevation anomaly of zero. We elaborate on this decision
 237 for each lake in more detail below and provide further commentary on preprocessing considerations in the
 238 discussion.

239 To invert the elevation-change data, we also must supply the approximate ice thickness \bar{H} , ice viscosity

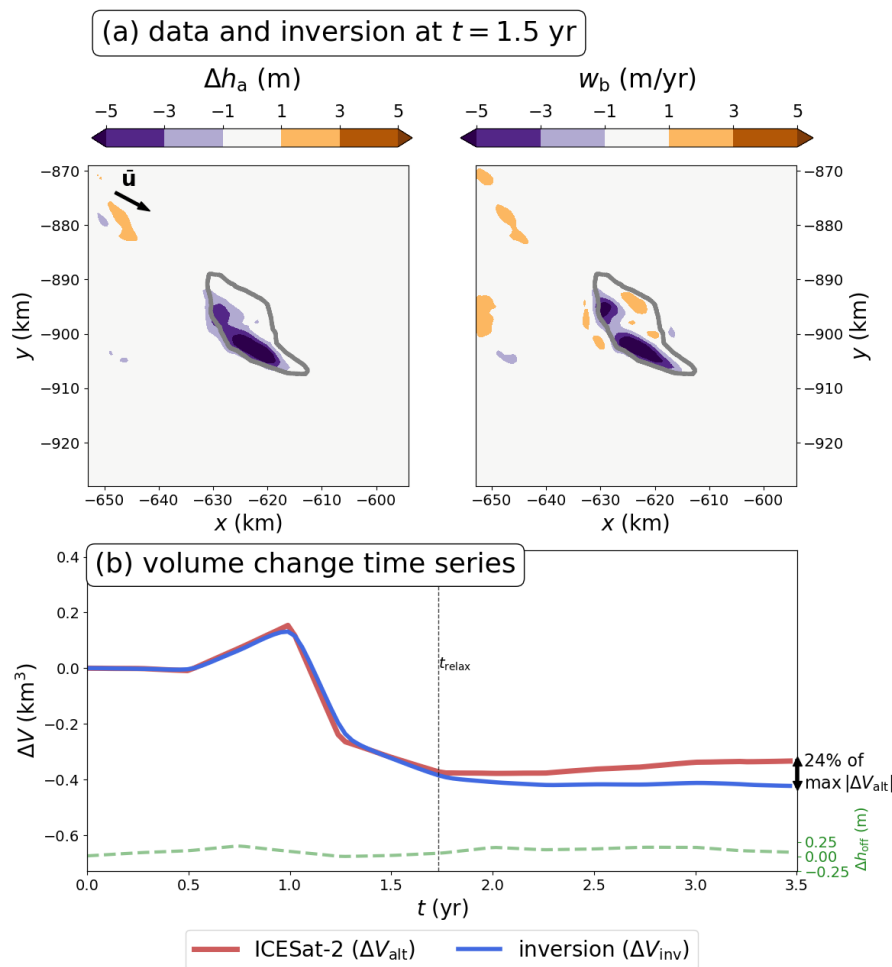


Fig. 5. Inversion results for subglacial lake Mac1. (a) Map-plane elevation anomaly and inversion at $t = 1.5$ yr. (b) Time series of the surface-derived volume change (ΔV_{alt}), the inversion-based volume change (ΔV_{inv}), and the off-lake component (Δh_{off}) that is removed prior to inversion. The gray contours in (a) and (b) show the boundaries used to compute the volume-change time series (Siegfried and Fricker, 2018). The ice flow direction is shown by the black arrow in (a). The maximum deviation between the surface-derived volume change and inversion is 0.09 km^3 , or 24% of the maximum amplitude of the surface-derived estimate. The parameters for this example are $\bar{H} = 926 \text{ m}$, $\bar{\eta} = 2.3 \times 10^{14} \text{ Pa s}$, $\bar{\beta} = 7.4 \times 10^{10} \text{ Pa s m}^{-1}$, $\bar{u} = 334 \text{ m yr}^{-1}$, and $\bar{v} = -178 \text{ m yr}^{-1}$. The viscous relaxation time associated with these parameters is $t_{\text{relax}} = 1.73 \text{ yr}$. See Movie S4 for an animation of the inversion over all time steps.

Table 1. Parameters used in the inversions of the Antarctic subglacial lakes shown in Figure 1. Data sources are described in the “Data and Preprocessing” section.

Parameter	units	Mac1	SLM	Slessor ₂₃	Thw ₁₇₀	Byrd _{s10}
\bar{H} : ice thickness	m	926	1003	1735	2558	2676
$\bar{\eta}$: ice viscosity	Pa s ($\times 10^{14}$)	2.3	2.2	2.4	5.7	50.0
$\bar{\beta}$: basal drag coefficient	Pa s m ⁻¹ ($\times 10^{10}$)	7.4	37.0	2.7	1.3	14.0
\bar{u} : surface velocity (x)	m yr ⁻¹	334	172	-141	-130	-9.4
\bar{v} : surface velocity (y)	m yr ⁻¹	-178	-65	-146	-78	-9.8

240 $\bar{\eta}$, basal drag coefficient $\bar{\beta}$, and horizontal ice velocity $\bar{\mathbf{u}} = [\bar{u}, \bar{v}]^T$ that describe the reference ice-flow state
 241 (Figure 2). The viscosity and basal drag estimates are derived from the inversions presented in Arthern and
 242 others (2015), which relied on the ALBMAP ice thickness (Le Brocq and others, 2010) and the MEaSURES
 243 InSAR-Based Antarctic Ice Velocity Map (Version 1) (Rignot and others, 2011; Mouginot and others, 2012).
 244 However, we obtain horizontal surface velocity from the MEaSURES Phase-Based Antarctic Ice Velocity
 245 Map (Version 1) (Mouginot and others, 2019a,b) and ice thickness from MEaSURES BedMachine Antarctica
 246 (Version 3) (Morlighem and others, 2020; Morlighem, 2022) for greater compatibility with the ICESat-2
 247 epoch. All parameter values are obtained by averaging these data over the extent of the computational
 248 domain. The parameter values for each example are reported in Table 1 and the figure captions. To define
 249 the boundaries B in the volume estimation equations (21) and (22), we use the latest subglacial boundary
 250 inventory (Siegfried and Fricker, 2018), which is a compilation of static active subglacial lake outlines from
 251 a variety of sources that used mixed delineation methods.

252 ICESAT-2 EXAMPLES

253 Next, we will invert ICESat-2 data (ATL15 gridded elevation-change product) for the subglacial lakes
 254 shown in Figure 1: Lake Mac1 beneath the MacAyeal Ice Stream (e.g., Fricker and others, 2010; Siegfried
 255 and Fricker, 2018, 2021), Mercer Subglacial Lake at the confluence of Mercer Ice Stream and Whillans
 256 Ice Stream (e.g., Fricker and others, 2007; Siegfried and Fricker, 2018, 2021; Siegfried and others, 2023),
 257 Slessor₂₃ beneath Slessor Glacier (Siegfried and Fricker, 2018; Siegfried and others, 2021), Thw₁₇₀ beneath
 258 Thwaites Glacier (Smith and others, 2017; Hoffman and others, 2020) and Byrd_{s10} beneath Byrd Glacier
 259 in East Antarctica (Smith and others, 2009; Wright and others, 2014). These lakes have been the sub-

260 ject of numerous previous investigations and represent a wide range of filling-draining patterns, physical
261 conditions, and locations across the Antarctic Ice Sheet (Table 1). For these examples, it is important to
262 consider the reference time t_{ref} used to define the elevation anomaly in equation (23). We base our choices
263 on the lake activity leading up to the ICESat-2 epoch. For example, subglacial lake Mac1 showed little
264 activity since the beginning of the ICESat-2 epoch in 2018 (Siegfried and Fricker, 2021), suggesting that the
265 initial time in the ATL15 data is an appropriate choice of reference time. For Mac1, there is a maximum
266 discrepancy of $\sim 0.12 \text{ km}^3$ between the surface-based and inversion-based volume-change estimates, or 24%
267 of the maximum amplitude of the surface-derived estimate (Figure 5).

268 We also show inversions of Mercer Subglacial Lake (SLM), which displays multiple oscillations over the
269 ICESat-2 period (Figure 6). We set the reference time to be $t = 1.3 \text{ yr}$ after the initial time (i.e. around
270 the second peak in the time series), as this more closely corresponds to the long-term mean of Mercer
271 Subglacial Lake's oscillation pattern (Siegfried and Fricker, 2021). For this example, we find a maximum
272 discrepancy of $\sim 0.05 \text{ km}^3$ between the surface-based and inversion-based volume-change estimates, or 19%
273 of the maximum amplitude of the surface-derived estimate.

274 We also invert elevation anomalies from Slessor Glacier (lake Slessor₂₃) and Thwaites Glacier (lake
275 Thw₁₇₀). Slessor₂₃ shows a discrepancy of $\sim 0.52 \text{ km}^3$ between the volume-change estimates, which is
276 62% of the maximum amplitude of the surface-derived estimate (Figure 7). Thw₁₇₀ also shows a large
277 discrepancy of $\sim 0.21 \text{ km}^3$, or 49% of the maximum in the altimetry-based estimate (Figure 8). For
278 Slessor₂₃, the initial time in the ICESat-2 data appears to be close to the midpoint of a filling stage, so
279 this reference time seems appropriate for defining the elevation anomaly (Siegfried and Fricker, 2018). On
280 the other hand, Thw₁₇₀ appears to be coming out of a quiescent post-drainage period at the beginning of
281 the ICESat-2 period, so choosing the correct reference time is more ambiguous in this case (Hoffman and
282 others, 2020; Malczyk and others, 2020). For example, setting the reference time to $t = 1.5 \text{ yr}$ instead
283 results in a maximum discrepancy of $\sim 0.075 \text{ km}^3$ between the volume-change estimates for the Thw₁₇₀
284 inversion. This discrepancy arises because the magnitude of the elevation-change anomaly is diminished
285 when choosing the different reference time and less of the signal is attributed to the basal forcing. We
286 quantify the sensitivity to the reference time more thoroughly in Appendix A and highlight the main issues
287 in the discussion.

288 The common theme of the preceding examples is that they have ice viscosities on the order of $\bar{\eta} = 10^{14}$
289 Pa s (Table 1) and volume-change discrepancies that are at least $\sim 20\%$ of the maximum of the altimetry-

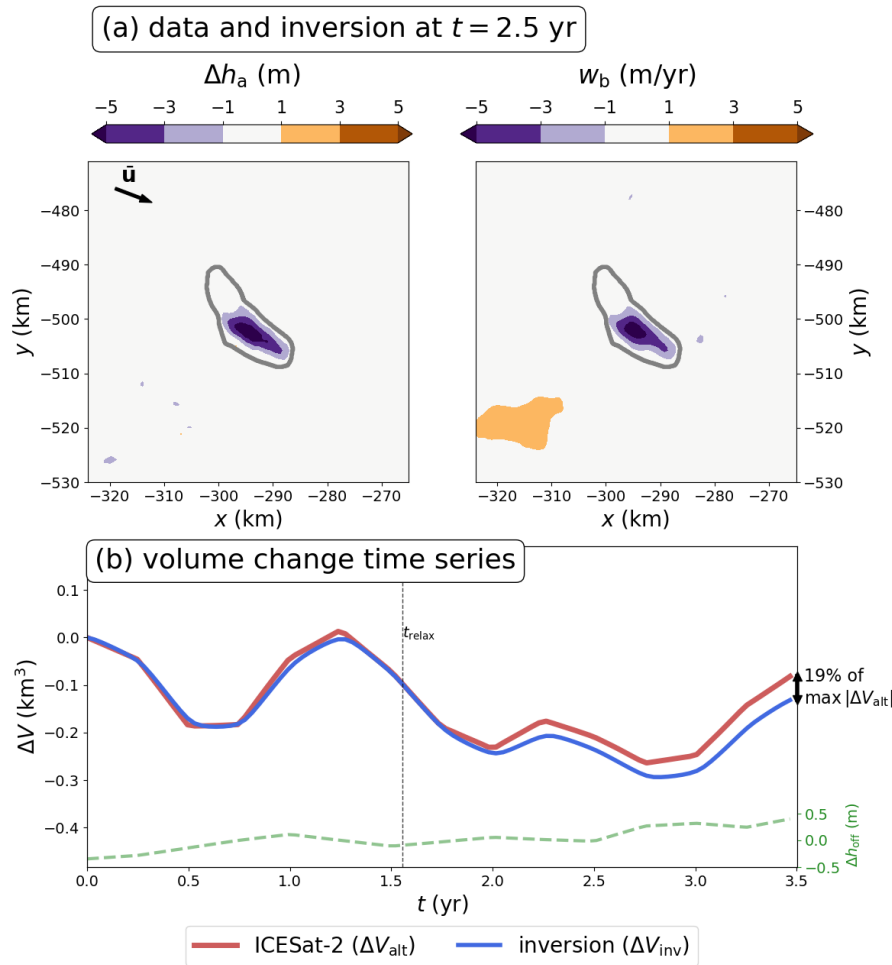


Fig. 6. Inversion results for Mercer Subglacial Lake (SLM in Figure 1). (a) Map-plane elevation anomaly and inversion at $t = 2.5$ yr. (b) Time series of the surface-derived volume change (ΔV_{alt}), the inversion-based volume change (ΔV_{inv}), and the off-lake component (Δh_{off}) that is removed prior to inversion. The gray contours in (a) and (b) show the boundaries used to compute the volume-change time series (Siegfried and Fricker, 2018). The ice flow direction is shown by the black arrow in (a). The maximum deviation between the surface-derived volume change and inversion in (b) is 0.05 km^3 , or 19% of the maximum amplitude of the surface-derived estimate. The parameters for this example are $\bar{H} = 1003 \text{ m}$, $\bar{\eta} = 2.2 \times 10^{14} \text{ Pa s}$, $\bar{\beta} = 3.7 \times 10^{11} \text{ Pa s m}^{-1}$, $\bar{u} = 172 \text{ m yr}^{-1}$, and $\bar{v} = -65 \text{ m yr}^{-1}$. The viscous relaxation time associated with these parameters is $t_{\text{relax}} = 1.56 \text{ yr}$. See Movie S5 for an animation of the inversion over all time steps.

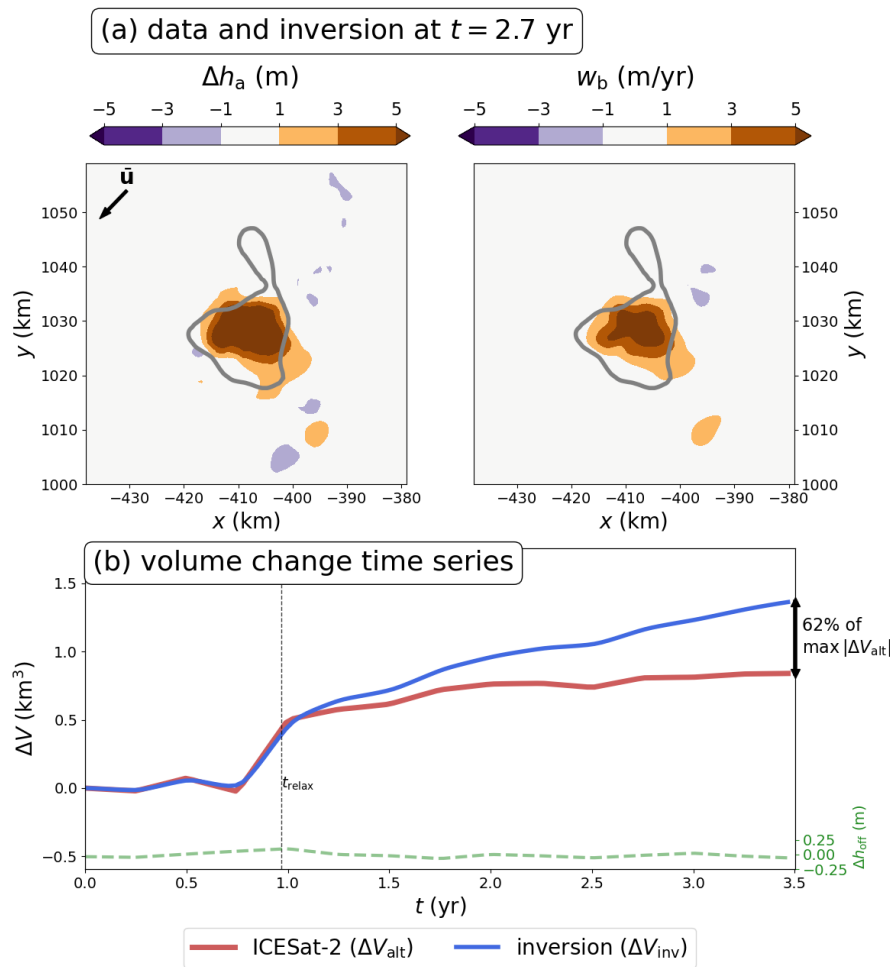


Fig. 7. Inversion results for subglacial lake Slessor₂₃. (a) Map-plane elevation anomaly and inversion at $t = 2.7$ yr. (b) Time series of the surface-derived volume change (ΔV_{ait}), the inversion-based volume change (ΔV_{inv}), and the off-lake component (Δh_{off}) that is removed prior to inversion. The gray contours in (a) and (b) show the boundaries used to compute the volume-change time series (Siegfried and Fricker, 2018). The ice flow direction is shown by the black arrow in (a). The maximum deviation between the altimetry-derived volume change and inversion in (b) is 0.52 km^3 , or 62% of the maximum amplitude of the surface-derived estimate. The parameters for this example are $\bar{H} = 1735 \text{ m}$, $\bar{\eta} = 2.4 \times 10^{14} \text{ Pa s}$, $\bar{\beta} = 2.7 \times 10^{10} \text{ Pa s m}^{-1}$, $\bar{u} = -141 \text{ m yr}^{-1}$, and $\bar{v} = -146 \text{ m yr}^{-1}$. The viscous relaxation time associated with these parameters is $t_{\text{relax}} = 0.97 \text{ yr}$. See Movie S6 for an animation of the inversion over all time steps.

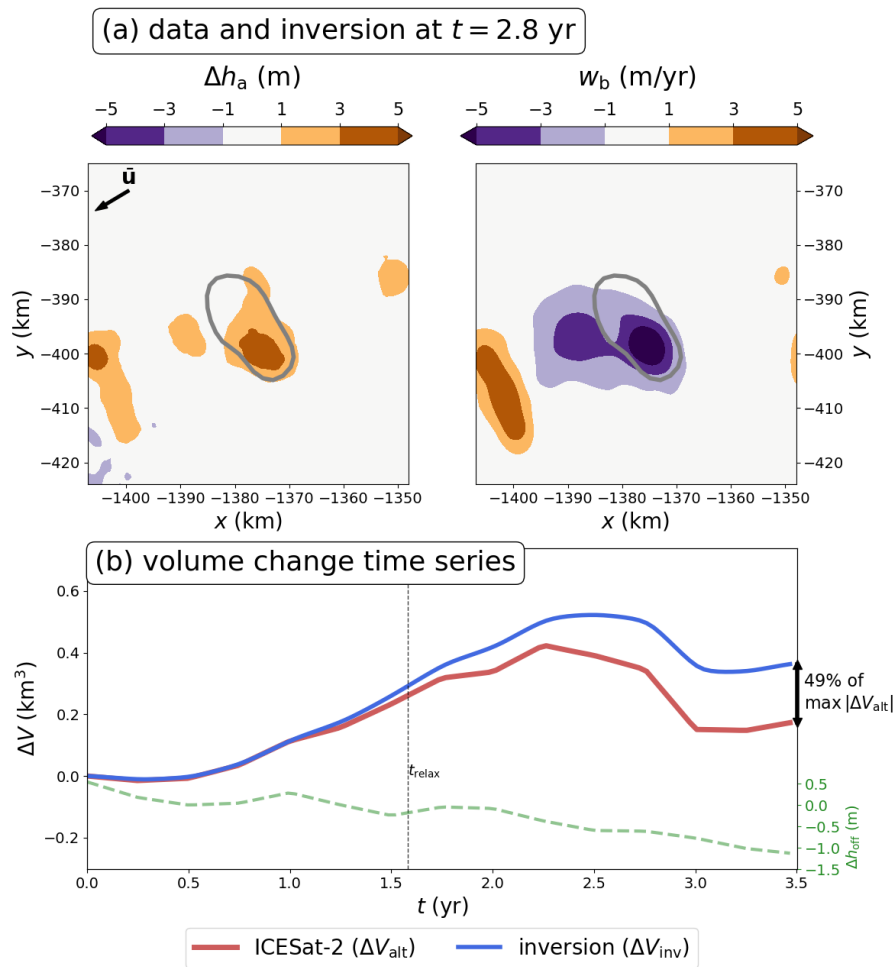


Fig. 8. Inversion results for subglacial lake Thw₁₇₀. (a) Map-plane elevation anomaly and inversion at $t = 2.8$ yr. (b) Time series of the surface-derived volume change (ΔV_{alt}), the inversion-based volume change (ΔV_{inv}), and the off-lake component (Δh_{off}) that is removed prior to inversion. The gray contours in (a) and (b) show the boundaries used to compute the volume-change time series (Smith and others, 2017). The ice flow direction is shown by the black arrow in (a). The maximum deviation between the altimetry-derived volume change and inversion is 0.21 km^3 , or 49% of the maximum amplitude of the surface-derived estimate. The parameters for this example are $\bar{H} = 2558$ m, $\bar{\eta} = 5.7 \times 10^{14}$ Pa s, $\bar{\beta} = 1.3 \times 10^{10}$ Pa s m^{-1} , $\bar{u} = -130$ m yr^{-1} , and $\bar{v} = -78$ m yr^{-1} . The viscous relaxation time associated with these parameters is $t_{\text{relax}} = 1.58$ yr. See Movie S7 for an animation of the inversion over all time steps.

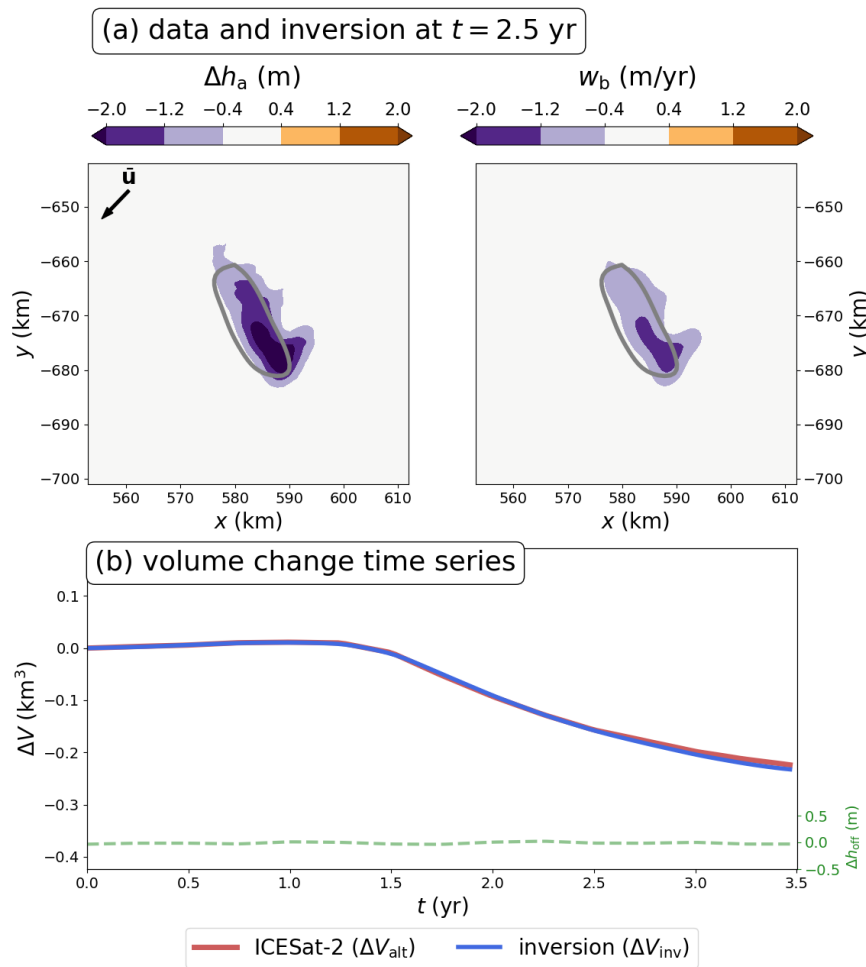


Fig. 9. Inversion results for subglacial lake Byrd_{s10}. (a) Map-plane elevation anomaly and inversion at $t = 2.5$ yr. (b) Time series of the surface-derived volume change (ΔV_{alt}), the inversion-based volume change (ΔV_{inv}), and the off-lake component (Δh_{off}) that is removed prior to inversion. The gray contours in (a) and (b) show the boundaries used to compute the volume-change time series. The ice flow direction is shown by the black arrow in (a). The maximum deviation between the altimetry-derived volume change and inversion is $9 \times 10^{-3} \text{ km}^3$, or 4% of the maximum amplitude of the surface-derived estimate. The parameters for this example are $\bar{H} = 2676 \text{ m}$, $\bar{\eta} = 5 \times 10^{15} \text{ Pa s}$, $\bar{\beta} = 1.4 \times 10^{11} \text{ Pa s m}^{-1}$, $\bar{u} = -9.4 \text{ m yr}^{-1}$, and $\bar{v} = -9.8 \text{ m yr}^{-1}$. The viscous relaxation time associated with these parameters is $t_{\text{relax}} = 13 \text{ yr}$. See Movie S7 for an animation of the inversion over all time steps. See Movie S8 for an animation of the inversion over all time steps.

290 based estimate (Figures 5-8). At higher viscosity values, the volume-change discrepancies diminish over
291 the current ICESat-2 time period. For example, the results for subglacial lake Byrd_{s10} show negligible
292 discrepancy between the surface-based and inversion-based volume estimates (Figure 9). This lack of
293 discrepancy arises because the ice over this lake has a viscosity of $\bar{\eta} = 5 \times 10^{15}$ Pa s, an order of magnitude
294 higher than the preceding ICESat-2 examples. In this case, the surface and basal motion correspond more
295 closely because the viscous relaxation time, $t_{\text{relax}} = 13$ yr, is much longer than the current ICESat-2 time
296 span. However, over decadal timescales larger discrepancies are still possible for this parameter regime
297 (e.g., Figure 3) unless the lake oscillation period is small compared to the relaxation time (Stubblefield and
298 others, 2021a).

299 DISCUSSION

300 Several practical and technical challenges are worth considering when applying the inverse method. From
301 a practical viewpoint, the primary challenge is deriving the elevation anomaly from the altimetry data. For
302 example, the inversion results may be sensitive to the details of how any regional thickening or thinning
303 trends are separated from the lake-related elevation changes (Fricker and Scambos, 2009; Smith and others,
304 2009; Siegfried and Fricker, 2018, 2021). The reference elevation profile that is used to define the elevation
305 anomaly from the data can also influence the inversion results, as we discussed in the case of subglacial lake
306 Thw₁₇₀. Likewise, choosing an appropriate reference elevation profile may be difficult when the ice-sheet
307 surface profile is heavily textured or the initial time in the data is during a volume-change event. In the
308 latter case, we have relied on records of lake oscillations from previous satellite altimetry missions to choose
309 appropriate reference times (Siegfried and Fricker, 2018, 2021). In Appendix A, we quantify the sensitivity
310 of inversion results to the choice of reference time for the synthetic data (Figure 10) and Thw₁₇₀ (Figure
311 11). The results highlight the importance of carefully considering the reference time or elevation profile
312 that is used to define the elevation-change anomaly (Appendix A). We leave further exploration of the
313 sensitivity of inversion results to preprocessing steps for future work.

314 The primary technical limitations of the perturbation-based inverse method is that the associated for-
315 ward models are inherently linear, posed on geometrically simple domains, and cannot deviate significantly
316 from the specified reference state. Although we have tested the validity of the method by inverting syn-
317 thetic data from a simple radially symmetric nonlinear problem (Figure 4), more complex problems could
318 require alternative methods. For example, a more accurate surrogate forward model could potentially be

319 obtained by training a neural network on a variety of nonlinear Stokes problems with different ice-flow
320 regimes (Jouvet, 2022; Jouvet and others, 2022).

321 We have also assumed that, to first order, the subglacial lakes do not coincide with reductions in
322 basal drag because the characteristic dipolar elevation anomaly associated with such slippery spots is
323 not discernible in the examples considered herein (e.g., Gudmundsson, 2003; Sergienko and others, 2007).
324 However, some large, inactive Antarctic subglacial lakes are known to coincide with slippery spots where
325 the ice surface is flat over most of the lake except on the upstream side where thinning occurs and the
326 downstream side where thickening occurs (Bell and others, 2006, 2007; Wright and Siegert, 2012). On
327 the other hand, several West Antarctic ice streams also have both subglacial lakes and localized regions
328 of anomalously high basal drag (sticky spots) in close proximity (Winberry and others, 2009; Sergienko
329 and Hulbe, 2011; Winberry and others, 2014; Siegfried and others, 2016). Joint inversion for basal vertical
330 velocity and basal drag anomalies may be tractable if an additional data source like high-resolution, time-
331 varying surface velocity is available. Simultaneously inverting for both perturbation types would be valuable
332 in regions containing both subglacial lake activity and basal drag anomalies.

333 In a similar vein, the inverse method assumes that reliable estimates of the (depth-averaged) ice viscosity
334 and basal drag coefficient are available. The results are sensitive to these parameters, as shown here
335 and in previous work (Stubblefield and others, 2021a). Estimates of the ice viscosity and basal drag
336 coefficient, which are obtained from ice-sheet modelling and inversion, come with uncertainty (Raymond
337 and Gudmundsson, 2009; Petra and others, 2014; Isaac and others, 2015). Accounting for uncertainty in
338 the inversion arising from these auxiliary parameters via formulation and solution of a Bayesian inverse
339 problem would be valuable (Babaniyi and others, 2021).

340 In this study, we have focused primarily on estimating subglacial water-volume changes. Another appli-
341 cation of the inverse method will be estimating subglacial lake shorelines or areal extent. Lake boundaries
342 are currently defined using ice-surface deformation extent to generate static lake boundaries (Siegfried and
343 Fricker, 2018); however, these static boundaries were generated using lower spatial resolution altimetry
344 instruments than are available today. This static view of lake boundaries has resulted in a number of lake
345 re-delineation attempts (e.g., Fricker and others, 2014; Siegfried and Fricker, 2018) and more recent sug-
346 gestions of time-variable lake boundaries (e.g., Neckel and others, 2021; Siegfried and Fricker, 2021). In our
347 study, it is clear that static subglacial lake boundaries do not dependably encompass the ICESat-2 surface
348 height change observations (Figures 5-9) likely because lake shorelines vary temporally. Additionally, re-

349 cent numerical modeling shows the surface-derived boundaries can have a larger areal extent than the true
350 lake boundary at the base (Stubblefield and others, 2021a). With our inverse method, we could attempt
351 to reconstruct subglacial shoreline evolution by tracking the areal extent of the basal forcing rather than
352 the surface deformation. Improving the accuracy of subglacial-lake shoreline estimates in this way could
353 be valuable for site selection in future subglacial drilling projects (Tulaczyk and others, 2014; Priscu and
354 others, 2021) and thereby provide stronger constraints on subglacial microbial and geochemical processes
355 (Christner and others, 2014; Achberger and others, 2016; Davis and others, 2023).

356 The inverse method could be extended to estimate other subglacial hydrological quantities besides
357 water-volume changes. For example, the temporal derivative of the volume change can be related to the
358 relative volumetric water discharge into (or out of) the lake (Evatt and Fowler, 2007). The water discharge
359 naturally appears in models of glacial lakes that are coupled to subglacial channel evolution (Fowler, 1999,
360 2009; Kingslake, 2015; Stubblefield and others, 2019; Jenson and others, 2022). Finally, an alternative
361 to prescribing a basal vertical velocity anomaly would have been prescribing a basal pressure anomaly.
362 Pressure perturbations could possibly be related to the subglacial effective pressure, the difference between
363 the cryostatic pressure and water pressure in the lake, since we have assumed that the pressure in the
364 reference state is cryostatic (cf. Evatt and Fowler, 2007). Estimating the effective pressure in this way
365 could be valuable for further constraining the physics of subglacial hydrological systems.

366 CONCLUSIONS

367 We have introduced and applied a simple inverse method for estimating the basal forcing associated
368 with subglacial lake activity from ice-sheet altimetry. We have provided some validation of the small-
369 perturbation approach by inverting synthetic data from a nonlinear subglacial lake model to obtain a
370 basal vertical velocity field and water-volume change time series that agree well with the nonlinear model.
371 We then applied the method to a collection of Antarctic subglacial lakes by inverting satellite altimetry
372 data from NASA's ICESat-2 mission. These results illustrate that there can be significant discrepancies
373 between surface-based estimation methods and the inversion due to the effects of viscous ice flow. The
374 inverse method provides a simple way to refine basal mass transport estimates derived from subglacial lakes
375 and further illuminate the physics of subglacial hydrological systems with satellite altimetry.

376 SUPPLEMENTARY MATERIAL

377 A link to the Supplementary material (Movies S1-S8 showing animations of Figures 3-9) will be placed
378 here.

379 DATA

380 All data used in this study are openly available:

381 ICESat-2 ATL15, Version 2 (<https://doi.org/10.5067/ATLAS/ATL15.002>),
382 WAVI ice-sheet model output (<https://doi.org/10.5285/5F0AC285-CCA3-4A0E-BCBC-D921734395AB>),
383 MEaSURES Phase-Based Antarctica Ice Velocity Map, Version 1 (<https://doi.org/10.5067/PZ3NJ5RXXRH10>),
384 MEaSURES BedMachine Antarctica, Version 3 (<https://doi.org/10.5067/FPSU0V1MWUB6>),
385 Subglacial lake inventory from Siegfried and Fricker (2018) (<https://doi.org/10.5281/zenodo.4914107>).

386 The code used to produce all results is openly available and the repository will be archived with Zenodo
387 upon acceptance (<https://github.com/agstub/lake-altimetry-inversions>).

388 ACKNOWLEDGEMENTS

389 A.G.S. thanks Jonathan Kingslake, Meredith Nettles, Ian Hewitt, and Brent Minchew for discussions
390 about the inverse problem. A.G.S. was supported by NSF (2012958). C.R.M. was supported by NSF
391 (2012958); ARO (78811EG); and NASA (80NSSC21M0329). M.R.S. and W.S. supported by NASA
392 (80NSSC21K0912).

393 REFERENCES

394 Achberger AM, Christner BC, Michaud AB, Priscu JC, Skidmore ML, Vick-Majors TJ, Adkins W, Anandakrishnan
395 S, Barbante C, Barcheck G, Beem L, Behar A, Beitch M, Bolsey R, Branecky C, Carter S, Christianson K, Edwards
396 R, Fisher A, Fricker H, Foley N, Guthrie B, Hodson T, Jacobel R, Kelley S, Mankoff K, McBryan E, Mikucki J,
397 Mitchell A, Powell R, Purcell A, Sampson D, Scherer R, Sherve J, Siegfried M and Tulaczyk S (2016) Microbial
398 community structure of subglacial Lake Whillans, West Antarctica. *Frontiers in Microbiology*, **7**(SEP), 1–13, ISSN
399 1664302X (doi: 10.3389/fmicb.2016.01457)

400 Arthern RJ, Hindmarsh RC and Williams CR (2015) Flow speed within the Antarctic ice sheet and its controls
401 inferred from satellite observations. *Journal of Geophysical Research: Earth Surface*, **120**(7), 1171–1188

- 402 Atkinson K and Han W (2009) *Theoretical numerical analysis*, volume 39. Springer, 3 edition
- 403 Babaniyi O, Nicholson R, Villa U and Petra N (2021) Inferring the basal sliding coefficient field for the stokes ice
404 sheet model under rheological uncertainty. *The Cryosphere*, **15**(4), 1731–1750
- 405 Balise MJ and Raymond CF (1985) Transfer of basal sliding variations to the surface of a linearly viscous glacier.
406 *Journal of Glaciology*, **31**(109), 308–318
- 407 Bell RE, Studinger M, Fahnestock MA and Shuman CA (2006) Tectonically controlled subglacial lakes on the flanks
408 of the Gamburtsev Subglacial Mountains, East Antarctica. *Geophysical Research Letters*, **33**(2)
- 409 Bell RE, Studinger M, Shuman CA, Fahnestock MA and Joughin I (2007) Large subglacial lakes in East Antarctica
410 at the onset of fast-flowing ice streams. *Nature*, **445**(7130), 904–907, ISSN 14764687 (doi: 10.1038/nature05554)
- 411 Bowling J, Livingstone S, Sole A and Chu W (2019) Distribution and dynamics of Greenland subglacial lakes. *Nature*
412 *communications*, **10**(1), 1–11
- 413 Budd W (1970) Ice flow over bedrock perturbations. *Journal of Glaciology*, **9**(55), 29–48
- 414 Christner BC, Priscu JC, Achberger AM, Barbante C, Carter SP, Christianson K, Michaud AB, Mikucki JA,
415 Mitchell AC, Skidmore ML and others (2014) A microbial ecosystem beneath the West Antarctic ice sheet. *Nature*,
416 **512**(7514), 310–313
- 417 Cuffey KM and Paterson WSB (2010) *The physics of glaciers*. Academic Press
- 418 Davis CL, Venturelli RA, Michaud AB, Hawkings JR, Achberger AM, Vick-Majors TJ, Rosenheim BE, Dore JE,
419 Steigmeyer A, Skidmore ML and others (2023) Biogeochemical and historical drivers of microbial community
420 composition and structure in sediments from Mercer Subglacial Lake, West Antarctica. *ISME communications*,
421 **3**(1), 8
- 422 Evatt GW and Fowler AC (2007) Cauldron subsidence and subglacial floods. *Annals of Glaciology*, **45**, 163–168,
423 ISSN 02603055 (doi: 10.3189/172756407782282561)
- 424 Fowler A (1999) Breaking the seal at Grímsvötn, Iceland. *Journal of Glaciology*, **45**(151), 506–516
- 425 Fowler A (2009) Dynamics of subglacial floods. *Proceedings of the Royal Society A: Mathematical, Physical and*
426 *Engineering Sciences*, **465**(2106), 1809–1828
- 427 Fricker HA and Scambos T (2009) Connected subglacial lake activity on lower Mercer and Whillans Ice
428 Streams, West Antarctica, 2003–2008. *Journal of Glaciology*, **55**(190), 303–315, ISSN 00221430 (doi:
429 10.3189/002214309788608813)

- 430 Fricker HA, Scambos T, Bindschadler R and Padman L (2007) An active subglacial water system in West Antarctica
431 mapped from space. *Science*, **315**(5818), 1544–1548
- 432 Fricker HA, Scambos T, Carter S, Davis C, Haran T and Joughin I (2010) Synthesizing multiple remote-sensing
433 techniques for subglacial hydrologic mapping: application to a lake system beneath MacAyeal Ice Stream, West
434 Antarctica. *Journal of Glaciology*, **56**(196), 187–199
- 435 Fricker HA, Carter SP, Bell RE and Scambos T (2014) Active lakes of Recovery Ice Stream, East Antarc-
436 tica: a bedrock-controlled subglacial hydrological system. *Journal of Glaciology*, **60**(223), 1015–1030 (doi:
437 10.3189/2014JoG14J063)
- 438 Fricker HA, Siegfried MR, Carter SP and Scambos TA (2016) A decade of progress in observing and modeling
439 Antarctic subglacial water systems. *Philosophical Transactions of the Royal Society A: Mathematical, Physical
440 and Engineering Sciences*, **374**(2059), ISSN 1364503X (doi: 10.1098/rsta.2014.0294)
- 441 Glen JW (1955) The creep of polycrystalline ice. *Proceedings of the Royal Society of London. Series A. Mathematical
442 and Physical Sciences*, **228**(1175), 519–538
- 443 Goldberg D, Heimbach P, Joughin I and Smith B (2015) Committed retreat of smith, pope, and kohler glaciers over
444 the next 30 years inferred by transient model calibration. *The Cryosphere*, **9**(6), 2429–2446
- 445 Gray L, Joughin I, Tulaczyk S, Spikes VB, Bindschadler R and Jezek K (2005) Evidence for subglacial water transport
446 in the West Antarctic Ice Sheet through three-dimensional satellite radar interferometry. *Geophysical Research
447 Letters*, **32**(3), L03501, ISSN 0094-8276
- 448 Greve R and Blatter H (2009) *Dynamics of ice sheets and glaciers*. Springer Science & Business Media
- 449 Gudmundsson GH (2003) Transmission of basal variability to a glacier surface. *Journal of Geophysical Research:
450 Solid Earth*, **108**(B5)
- 451 Gudmundsson GH and Raymond M (2008) On the limit to resolution and information on basal properties obtainable
452 from surface data on ice streams. *The Cryosphere*, **2**(2), 167–178
- 453 Hanke M (2017) *A Taste of Inverse Problems: Basic Theory and Examples*. SIAM
- 454 Hoffman AO, Christianson K, Shapero D, Smith BE and Joughin I (2020) Brief communication: Heterogenous
455 thinning and subglacial lake activity on Thwaites Glacier, West Antarctica. *The Cryosphere*, **14**(12), 4603–4609
- 456 Hutter K, Legerer F and Spring U (1981) First-order stresses and deformations in glaciers and ice sheets. *Journal of
457 Glaciology*, **27**(96), 227–270

- 458 Isaac T, Petra N, Stadler G and Ghattas O (2015) Scalable and efficient algorithms for the propagation of uncertainty
459 from data through inference to prediction for large-scale problems, with application to flow of the Antarctic ice
460 sheet. *Journal of Computational Physics*, **296**, 348–368
- 461 Jenson A, Amundson JM, Kingslake J and Hood E (2022) Long-period variability in ice-dammed glacier outburst
462 floods due to evolving catchment geometry. *The Cryosphere*, **16**(1), 333–347
- 463 Jouvét G (2022) Inversion of a Stokes glacier flow model emulated by deep learning. *Journal of Glaciology*, 1–14
- 464 Jouvét G, Cordonnier G, Kim B, Lüthi M, Vieli A and Aschwanden A (2022) Deep learning speeds up ice flow
465 modelling by several orders of magnitude. *Journal of Glaciology*, **68**(270), 651–664
- 466 Kingslake J (2015) Chaotic dynamics of a glaciodynamic model. *Journal of Glaciology*, **61**(227), 493–502
- 467 Larour E, Utke J, Csatho B, Schenk A, Seroussi H, Morlighem M, Rignot E, Schlegel N and Khazendar A (2014)
468 Inferred basal friction and surface mass balance of the Northeast Greenland Ice Stream using data assimilation
469 of ICESat (Ice Cloud and land Elevation Satellite) surface altimetry and ISSM (Ice Sheet System Model). *The
470 Cryosphere*, **8**(6), 2335–2351
- 471 Le Brocq AM, Payne AJ and Vieli A (2010) An improved Antarctic dataset for high resolution numerical ice sheet
472 models (ALBMAP v1). *Earth System Science Data*, **2**(2), 247–260
- 473 Livingstone SJ, Sole AJ, Storrar RD, Harrison D, Ross N and Bowling J (2019) Brief communication: Subglacial
474 lake drainage beneath Isunguata Sermia, West Greenland: Geomorphic and ice dynamic effects. *The Cryosphere*,
475 **13**(10), 2789–2796
- 476 Livingstone SJ, Li Y, Rutishauser A, Sanderson RJ, Winter K, Mikucki JA, Björnsson H, Bowling JS, Chu W, Dow
477 CF and others (2022) Subglacial lakes and their changing role in a warming climate. *Nature Reviews Earth &
478 Environment*, **3**(2), 106–124
- 479 Malczyk G, Gourmelen N, Goldberg D, Wuite J and Nagler T (2020) Repeat subglacial lake drainage and filling
480 beneath Thwaites Glacier. *Geophysical Research Letters*, **47**(23), e2020GL089658
- 481 Markus T, Neumann T, Martino A, Abdalati W, Brunt K, Csatho B, Farrell S, Fricker H, Gardner A, Harding D
482 and others (2017) The Ice, Cloud, and land Elevation Satellite-2 (ICESat-2): science requirements, concept, and
483 implementation. *Remote sensing of environment*, **190**, 260–273
- 484 Morlighem M (2022) Measures bedmachine antarctica, version 3 (doi: 10.5067/FPSU0V1MWUB6)
- 485 Morlighem M, Rignot E, Binder T, Blankenship D, Drews R, Eagles G, Eisen O, Ferraccioli F, Forsberg R, Fretwell
486 P and others (2020) Deep glacial troughs and stabilizing ridges unveiled beneath the margins of the Antarctic ice
487 sheet. *Nature Geoscience*, **13**(2), 132–137

- 488 Mosbeux C, Gillet-Chaulet F and Gagliardini O (2016) Comparison of adjoint and nudging methods to initialise ice
489 sheet model basal conditions. *Geoscientific Model Development*, **9**(7), 2549–2562
- 490 Mouginot J, Scheuchl B and Rignot E (2012) Mapping of ice motion in Antarctica using synthetic-aperture radar
491 data. *Remote Sensing*, **4**(9), 2753–2767
- 492 Mouginot J, Rignot E and B S (2019a) Measures phase-based antarctica ice velocity map, version 1 (doi:
493 10.5067/PZ3NJ5RXHR10)
- 494 Mouginot J, Rignot E and Scheuchl B (2019b) Continent-wide, interferometric SAR phase, mapping of Antarctic ice
495 velocity. *Geophysical Research Letters*, **46**(16), 9710–9718
- 496 Neckel N, Franke S, Helm V, Drews R and Jansen D (2021) Evidence of Cascading Subglacial Water Flow at
497 Jutulstraumen Glacier (Antarctica) Derived From Sentinel-1 and ICESat-2 Measurements. *Geophysical Research*
498 *Letters*, **48**(20), e2021GL094472
- 499 Petra N, Martin J, Stadler G and Ghattas O (2014) A computational framework for infinite-dimensional Bayesian
500 inverse problems, Part II: Stochastic Newton MCMC with application to ice sheet flow inverse problems. *SIAM*
501 *Journal on Scientific Computing*, **36**(4), A1525–A1555
- 502 Priscu JC, Kalin J, Winans J, Campbell T, Siegfried MR, Skidmore M, Dore JE, Leventer A, Harwood DM, Duling
503 D and others (2021) Scientific access into Mercer Subglacial Lake: scientific objectives, drilling operations and
504 initial observations. *Annals of Glaciology*, **62**(85-86), 340–352
- 505 Raymond MJ and Gudmundsson GH (2009) Estimating basal properties of ice streams from surface measurements:
506 a non-linear Bayesian inverse approach applied to synthetic data. *The Cryosphere*, **3**(2), 265–278
- 507 Rignot E, Mouginot J and Scheuchl B (2011) Ice flow of the Antarctic ice sheet. *Science*, **333**(6048), 1427–1430
- 508 Scambos TA, Berthier E and Shuman CA (2011) The triggering of subglacial lake drainage during rapid glacier
509 drawdown: Crane Glacier, Antarctic Peninsula. *Annals of Glaciology*, **52**(59), 74–82, ISSN 02603055 (doi:
510 10.3189/172756411799096204)
- 511 Sergienko O (2012) The effects of transverse bed topography variations in ice-flow models. *Journal of Geophysical*
512 *Research: Earth Surface*, **117**(F3)
- 513 Sergienko OV and Hulbe CL (2011) ‘Sticky spots’ and subglacial lakes under ice streams of the Siple Coast, Antarctica.
514 *Annals of Glaciology*, **52**(58), 18–22
- 515 Sergienko OV, MacAyeal DR and Bindschadler RA (2007) Causes of sudden, short-term changes in ice-stream surface
516 elevation. *Geophysical Research Letters*, **34**(22), 1–6, ISSN 00948276 (doi: 10.1029/2007GL031775)

- 517 Siegfried M and Fricker H (2021) Illuminating active subglacial lake processes with ICESat-2 laser altimetry. *Geo-*
518 *physical Research Letters*, **48**(14), e2020GL091089
- 519 Siegfried M, Venturelli R, Patterson M, Arnuk W, Campbell T, Gustafson C, Michaud A, Galton-Fenzi B, Hausner
520 M, Holzschuh S, Huber B, Mankoff K, Schroeder D, Summers P, Tyler S, Carter S, Fricker H, Harwood D, Leventer
521 A, Rosenheim B, Skidmore M, Priscu J and the SALSA Science Team (2023) The life and death of a subglacial
522 lake in West Antarctica. *Geology*, **51**(5), 434–438, ISSN 0091-7613 (doi: 10.1130/G50995.1)
- 523 Siegfried MR and Fricker HA (2018) Thirteen years of subglacial lake activity in Antarctica from multi-mission
524 satellite altimetry. *Annals of Glaciology*, **59**, 1–14, ISSN 0260-3055 (doi: 10.1017/aog.2017.36)
- 525 Siegfried MR, Fricker HA, Carter SP and Tulaczyk S (2016) Episodic ice velocity fluctuations triggered by
526 a subglacial flood in West Antarctica. *Geophysical Research Letters*, **43**(6), 2640–2648, ISSN 19448007 (doi:
527 10.1002/2016GL067758)
- 528 Siegfried MR, Schroeder DM, Sauthoff W and Smith B (2021) Investigating a large subglacial lake drainage in east
529 antarctica with ice-penetrating radar. In *SEG/AAPG/SEPM First International Meeting for Applied Geoscience*
530 *& Energy*, OnePetro
- 531 Smith B, Sutterley T, Dickinson S, Jelley B, Felikson D, Neumann TA, Fricker H, Gardner A, Padman L, Markus
532 T, Kurtz N, Bhardwaj S, Hancock D and Lee J (2022) ATLAS/ICESat-2 L3B Gridded Antarctic and Arctic Land
533 Ice Height Change, Version 2 (doi: 10.5067/ATLAS/ATL15.002)
- 534 Smith BE, Fricker HA, Joughin IR and Tulaczyk S (2009) An inventory of active subglacial lakes in Antarctica
535 detected by ICESat (2003–2008). *Journal of Glaciology*, **55**(192), 573–595
- 536 Smith BE, Gourmelen N, Huth A and Joughin I (2017) Connected subglacial lake drainage beneath Thwaites Glacier,
537 West Antarctica. *Cryosphere*, **11**(1), 451–467, ISSN 19940424 (doi: 10.5194/tc-11-451-2017)
- 538 Stadler G (2009) Elliptic optimal control problems with L1-control cost and applications for the placement of control
539 devices. *Computational Optimization and Applications*, **44**(2), 159
- 540 Stearns LA, Smith BE and Hamilton GS (2008) Increased flow speed on a large east antarctic outlet glacier caused
541 by subglacial floods. *Nature Geoscience*, **1**(12), 827–831, ISSN 17520894 (doi: 10.1038/ngeo356)
- 542 Stubblefield AG (2022) *Modelling the dynamics and surface expressions of subglacial water flow*. Ph.D. thesis,
543 Columbia University
- 544 Stubblefield AG, Creyts TT, Kingslake J and Spiegelman M (2019) Modeling oscillations in connected glacial lakes.
545 *Journal of Glaciology*, **65**(253), 745–758

- 546 Stubblefield AG, Creyts TT, Kingslake J, Siegfried MR and Spiegelman M (2021a) Surface Expression and Apparent
547 Timing of Subglacial Lake Oscillations Controlled by Viscous Ice Flow. *Geophysical Research Letters*, **48**(17),
548 e2021GL094658 (doi: <https://doi.org/10.1029/2021GL094658>), e2021GL094658 2021GL094658
- 549 Stubblefield AG, Spiegelman M and Creyts TT (2021b) Variational formulation of marine ice-sheet and subglacial-
550 lake grounding-line dynamics. *Journal of Fluid Mechanics*, **919**, A23 (doi: [10.1017/jfm.2021.394](https://doi.org/10.1017/jfm.2021.394))
- 551 Thorsteinsson T, Raymond CF, Gudmundsson GH, Bindschadler RA, Vornberger P and Joughin I (2003) Bed
552 topography and lubrication inferred from surface measurements on fast-flowing ice streams. *Journal of Glaciology*,
553 **49**(167), 481–490
- 554 Tulaczyk S, Mikucki JA, Siegfried MR, Priscu JC, Barcheck CG, Beem LH, Behar A, Burnett J, Christner BC, Fisher
555 AT, Fricker HA, Mankoff KD, Powell RD, Rack F, Sampson D, Scherer RP and Schwartz SY (2014) WISSARD
556 at Subglacial Lake Whillans, West Antarctica: Scientific operations and initial observations. *Annals of Glaciology*,
557 **55**(65), 51–58, ISSN 02603055 (doi: [10.3189/2014AoG65A009](https://doi.org/10.3189/2014AoG65A009))
- 558 Turcotte DL and Schubert G (2002) *Geodynamics*. Cambridge university press
- 559 Virtanen P, Gommers R, Oliphant TE, Haberland M, Reddy T, Cournapeau D, Burovski E, Peterson P, Weckesser
560 W, Bright J, van der Walt SJ, Brett M, Wilson J, Millman KJ, Mayorov N, Nelson ARJ, Jones E, Kern R,
561 Larson E, Carey CJ, Polat İ, Feng Y, Moore EW, VanderPlas J, Laxalde D, Perktold J, Cimrman R, Henriksen
562 I, Quintero EA, Harris CR, Archibald AM, Ribeiro AH, Pedregosa F, van Mulbregt P and SciPy 10 Contributors
563 (2020) SciPy 1.0: Fundamental Algorithms for Scientific Computing in Python. *Nature Methods*, **17**, 261–272 (doi:
564 [10.1038/s41592-019-0686-2](https://doi.org/10.1038/s41592-019-0686-2))
- 565 Vogel CR (2002) *Computational Methods for Inverse Problems*. Society for Industrial and Applied Mathematics (doi:
566 [10.1137/1.9780898717570](https://doi.org/10.1137/1.9780898717570))
- 567 Weertman J (1957) On the sliding of glaciers. *Journal of glaciology*, **3**(21), 33–38
- 568 Winberry JP, Anandakrishnan S and Alley RB (2009) Seismic observations of transient subglacial water-flow beneath
569 MacAyeal Ice Stream, West Antarctica. *Geophysical Research Letters*, **36**(11)
- 570 Winberry JP, Anandakrishnan S, Alley RB, Wiens DA and Pratt MJ (2014) Tidal pacing, skipped slips and the
571 slowdown of Whillans Ice Stream, Antarctica. *Journal of Glaciology*, **60**(222), 795–807
- 572 Wingham DJ, Siegert MJ, Shepherd A and Muir AS (2006) Rapid discharge connects Antarctic subglacial lakes.
573 *Nature*, **440**(7087), 1033–1036, ISSN 14764687 (doi: [10.1038/nature04660](https://doi.org/10.1038/nature04660))
- 574 Wright A and Siegert M (2012) A fourth inventory of Antarctic subglacial lakes. *Antarctic Science*, **24**(6), 659–664,
575 ISSN 09541020 (doi: [10.1017/S095410201200048X](https://doi.org/10.1017/S095410201200048X))

576 Wright A, Young D, Bamber J, Dowdeswell J, Payne A, Blankenship D and Siegert M (2014) Subglacial hydrological
577 connectivity within the Byrd Glacier catchment, East Antarctica. *Journal of Glaciology*, **60**(220), 345–352

578 APPENDIX A - SENSITIVITY TO REFERENCE TIME

579 As noted in the results and discussion, the primary challenge of applying the inverse method in practice is
580 defining the elevation-change anomaly from the data. We must choose a reference time t_{ref} to define the
581 anomaly through equation (23). To explore this sensitivity further, we inverted the synthetic data (Figure
582 3) after re-defining the anomaly to be zero at a range of incorrect reference times. The results show that
583 choosing an appropriate reference time has a strong influence on the validity of the inversion. Choosing
584 an incorrect reference time can cause significant deviations between the inversion and the true solution
585 (Figure 10).

586 We repeated the experiment by inverting the Thw₁₇₀ data after re-defining the anomaly to be zero at
587 a range of alternative reference times (Figure 11). We find that none of the options correspond exactly to
588 the altimetry-based estimate over the ICESat-2 time period, although the earlier reference times ($t_{\text{ref}} \leq 1$)
589 correspond more closely to the expected behavior of a lake undergoing a filling stage (e.g., Figure 3). Even
590 so, it not entirely clear based on previously published data which option is the most valid (Hoffman and
591 others, 2020). Further investigation to determine when local perturbations in glacier surface elevation reach
592 a viscously relaxed state in more complex settings (e.g., Thwaites Glacier) would be valuable.

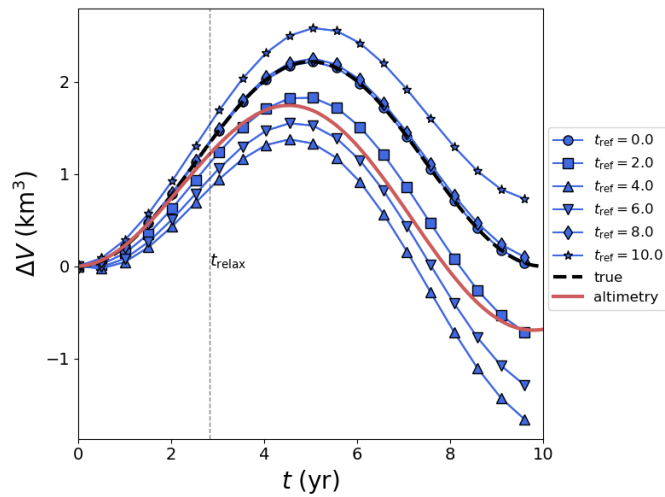


Fig. 10. Inversion of synthetic data from Figure 3 after redefining the reference time t_{ref} in equation (23) to a range of incorrect values. The correct reference time in this example is $t_{\text{ref}} = 0$. Significant deviations between the inversion and true solution can occur if an incorrect reference time is chosen.

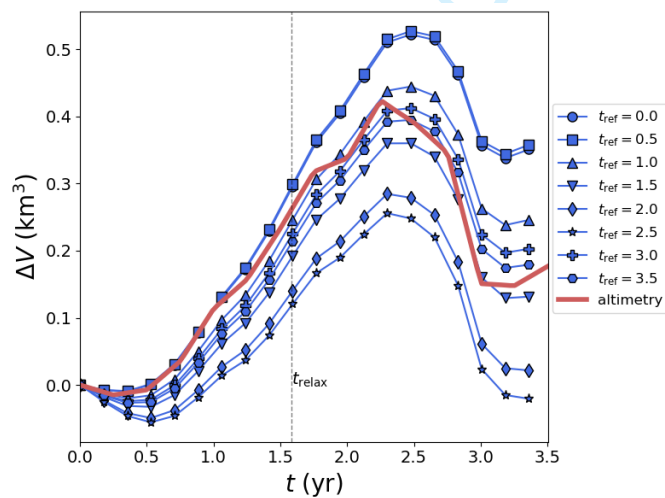


Fig. 11. Inversion of the Thw_{170} data from Figure 8 after redefining the reference time t_{ref} in equation (23) to a range of alternative values.